



# Spatio-temporal analysis of the sources and transformations of anthropogenic nitrogen in a highly degraded coastal basin in Southeast China

Shengwei Cao<sup>1,2</sup> · Yasong Li<sup>1,2</sup> · Qichen Hao<sup>1,2</sup> · Chunlei Liu<sup>1,2</sup> · Yuchen Zhu<sup>1,2</sup> · Zhenghong Li<sup>1,2</sup> · Ruoxi Yuan<sup>2</sup>

Received: 1 September 2022 / Accepted: 17 June 2023 / Published online: 4 July 2023

© The Author(s), under exclusive licence to Springer-Verlag GmbH Germany, part of Springer Nature 2023

## Abstract

Nitrogen transport from terrestrial to aquatic environments could cause water quality deterioration and eutrophication. By sampling in the high- and low-flow periods in a highly disturbed coastal basin of Southeast China, hydrochemical characteristics, nitrate stable isotope composition, estimation of potential nitrogen source input fluxes, and the Bayesian mixing model were combined to determine the sources and transformation of nitrogen. Nitrate was the main form of nitrogen. Nitrification, nitrate assimilation, and  $\text{NH}_4^+$  volatilization were the main nitrogen transformation processes, whereas denitrification was limited due to the high flow rate and unsuitable physicochemical properties. For both sampling periods, non-point source pollution from the upper to the middle reaches was the main source of nitrogen, especially in the high-flow period. In addition to synthetic fertilizer, atmospheric deposition and sewage and manure input were also major nitrate sources in the low-flow period. Hydrological condition was the main factor determining nitrate transformation in this coastal basin, despite the high degree of urbanization and the high volume of sewage discharge in the middle to the lower reaches. The findings of this study highlight that the control of agricultural non-point contamination sources is essential to pollution and eutrophication alleviation, especially for watersheds that receive high amounts of annual precipitation.

**Keywords** Non-point source pollution · Stable isotope · Nitrogen · Bayesian model · Coastal basin

---

Responsible Editor: V.V.S.S. Sarma

## Highlights

- Nitrification and assimilation were the main nitrogen transformation processes.
- The contribution of synthetic fertilizer increased toward the lower reach.
- Hydrological conditions determine nitrogen transformation in coastal watersheds.
- A high flow rate may mask the sources and transformation of nitrogen.
- Non-point sources were the main cause of nitrate pollution.

---

✉ Yasong Li  
liyason712@126.com

<sup>1</sup> Fujian Provincial Key Laboratory of Water Cycling and Eco-Geological Processes, Xiamen 361021, Fujian, China

<sup>2</sup> Institute of Hydrogeology and Environmental Geology, Chinese Academy of Geological Sciences, Shijiazhuang 050061, Hebei, China

## Introduction

Nitrogen transport from terrestrial to aquatic environments largely contributes to the nitrogen (N) amount in estuarine waters, leading to eutrophication, harmful algal blooms, and hypoxia (Richards et al. 2021). Coastal basins are the hot spot for rapid economic development; therefore, the environmental and ecological qualities of coastal basins largely rely on the fragile equilibrium between land and ocean interactions in the coastal zone and are particularly susceptible to the variations in hydrological conditions and human activities (Ye et al. 2017; Han and Currell 2022). This vulnerability is accentuated by the increasing anthropogenic pressure exerted on them (Bertrand et al. 2022). Such activities are often associated with point (e.g., municipal and industrial sewage leakages) and non-point source pollution (e.g., agricultural runoff and atmospheric deposition) that directly impact the environment quality (Botero-Acosta et al. 2019; Kibuye et al. 2020) and greatly alter the pool of carbon and nitrogen in coastal area (de la Reguera and Tully 2021).

As N does not behave conservatively in aquatic environments, determining the sources and transformation of N is still challenging, also because of the complex anthropogenic activities and hydrological conditions at catchment scale (Ding et al. 2015), which alter the composition and concentration of N via terrestrial input and internal retention (Yang and Toor 2016). In this context, the isotopic signatures of nitrate ( $\delta^{15}\text{N-NO}_3^-$  and  $\delta^{18}\text{O-NO}_3^-$ ) can provide valuable information on the sources and fate of N in aquatic environments (Kendall 1998; Yu et al. 2021). Different sources of N have distinct isotopic signatures, which can be used diagnostically to semi-quantify the relative importance of single N sources (Xue et al. 2009; Nestler et al. 2011).

Biological processes, such as nitrification, could lead to isotope fractionation; as the light isotope ( $^{14}\text{N}$ ) is preferentially used by microorganisms, depletion of  $\delta^{15}\text{N-NO}_3^-$  is likely to be observed during this process (Jacob et al. 2016). Laboratory studies have verified that, during nitrification, the conversion of ammonium to nitrate by microbial activities requires two oxygen atoms from water in the substrate and one oxygen atom from the atmosphere (Aleem et al. 1965; DiSpirito and Hooper 1986). In field conditions, due to the isotopic fraction caused by evaporation and respiration,  $\delta^{18}\text{O}$  in water and atmosphere could be higher than those in laboratory conditions. Thus,  $\delta^{18}\text{O}$  of newly microbially produced nitrate could be 5‰ higher than the theoretical value obtained in the laboratory (Kendall 1998). But, such deviation could not prevent  $\delta^{18}\text{N-NO}_3^-$  from being an effective tool to determine nitrogen sources and transformation.

By contrast, denitrification would cause an enrichment of  $\delta^{15}\text{N}$  and  $\delta^{18}\text{O}$  in residual nitrate at ratios between 1.3 and 2.1 (Archana et al. 2018; Zhang et al. 2018). Both denitrification and anaerobic ammonium oxidation can alleviate nitrate contamination by transforming it into harmless forms, such as  $\text{N}_2$  (Bernard-Jannin et al. 2017). Besides denitrification,  $\text{NO}_3^-$  assimilation by phytoplankton can also cause an increase in  $\delta^{15}\text{N-NO}_3^-$  and  $\delta^{18}\text{O-NO}_3^-$ , with ratios between these two isotopes close to 1.0 (Mohd Jani and Toor 2018; Yu et al. 2018). With the application of the nitrate dual-isotope technique in combination with physicochemical water quality data, precipitation data, hydrological data, land use data, and other tracers (e.g., boron isotopes, chloride), some authors have successfully determined the sources and transformation process of N in different ecosystems, such as river-aquifer system (Meghdadi and Javar 2018; Kwon et al. 2021), karst systems (Valiente et al. 2020), urban basin (Jin et al. 2018; Guo et al. 2021), and coastal basin (Chang et al. 2021).

The distribution and correlation between  $\delta^{15}\text{N-NO}_3^-$  and  $\delta^{18}\text{O-NO}_3^-$  could help to qualitatively determine the potential nitrate sources. However, it is important to acknowledge the limitations when discussing the uncertainty caused by isotope fractionation and mixing process of different nitrate

sources (Yu et al. 2021). This is due to the typical isotopic compositions of nitrate from different sources which can overlap, making it challenging to definitively differentiate the sources based solely on isotopic ratios, which may bring great uncertainties to the determination of sources.

The initial attempt to quantify the potential sources of nitrate in water relied on the simple linear mixing model to derive an analytical solution (Deutsch et al. 2006; Voss et al. 2006). However, this model proved inadequate in underdetermined systems where the number of potential sources exceeded the number of environmental tracers by two. IsoSource, an alternative approach, partially addresses this issue by providing distributions of feasible solutions through iterative calculations utilizing a “tolerance” term (Phillips and Gregg 2003). However, IsoSource is also based on the linear mixing model and only accepts mean values when inputting the isotopic compositions of potential sources, disregarding standard deviations or the “raw data” of isotopic compositions from potential sources; the outputs of IsoSources are based on the maximum likelihood estimation, providing point estimates without the analysis of associated probabilities and uncertainties.

Since the introduction of Bayesian mixing model framework, several packages have been developed to estimate the contribution of different sources to a mixture (Stock et al. 2014), such as SIAR (Parnell et al. 2013), MixSIR (Moore and Semmens 2008), and MixSIAR (Stock et al. 2014). These models use a Markov chain Monte Carlo (MCMC) algorithm, based on the input of mixtures’ isotope composition, assumed prior distribution of potential sources, the associated isotopic range of each sources, and isotope fractionation factors to quantitatively estimate the contribution of different nitrate sources to the mixture (i.e., water samples in our study). During the MCMC simulation process, the Bayesian mixing model generated a large number of posterior samples, which enable the estimation of uncertainties and credible interval of source estimations (Li et al. 2023).

Among the aforementioned packages developed based on the Bayesian mixing model framework, MixSIAR stands out by introducing a hierarchical structure. This feature enables the categorization of mixtures into different levels or groups, facilitating the analysis of nested relationships among different categories within the data. Additionally, MixSIAR incorporates the distinction between random effects and fixed effects for categorical variables. By considering random effects, MixSIAR can estimate varying effects across different categories, capturing the variability associated with each category. In contrast, fixed effects provide deterministic estimates, assuming a constant effect across all observations within the category. These unique features make MixSIAR a more powerful tool for exploring complex relationships and variations in source contributions compared to other

packages. However, to ensure that the Bayesian mixing models and hydrochemical analyses accurately reflect the characteristics of the watershed, it is necessary to compare the results estimated by considering the input fluxes of different nitrogen sources, while also taking into account the local socio-economic factors and human activities within the watershed (Kim et al. 2023).

The Jin River Basin is located in the coastal area of Southeast China and contains the Shanmei Reservoir, which not only serves as the main water supply and flood control facility for the downstream Quanzhou City but also supplies water to Kinmen County, which is managed by the Taiwan Region. Thus, protecting the aquatic environment in the Jin River Basin has both ecological and political significance. Identification of N sources and transformation is an important step in maintaining and restoring the aquatic environment of this coastal basin. In this context, our objectives were to (1) investigate the variations in N composition and water quality at the longitudinal scale from freshwater to seawater, (2) distinguish the sources of nitrate using stable isotopes of  $\text{NO}_3^-$  and the Bayesian mixing model, and (3) discuss the biogeochemical mechanisms of nitrate transport under the influences of terrestrial nutrient export, providing evidence for microbial N transformations in the Jin River Basin.

## Materials and methods

### Study area

The Jin River Basin is located in Fujian Province, Southeast China, and covers an area of 5692 km<sup>2</sup>. Considering the limited funds and the difficulty to obtain water samples at the basin scale, we selected the Dong River, which is the main tributary of the Jin River and converges with the Xi River at the lower reach of the Jin River (our study area is about 2500 km<sup>2</sup>). The distance of this confluence to Quanzhou Bay, which is a semi-closed bay and the outlet of the Jin River, is about 28 km. The Shanmei Reservoir, a large reservoir in Quanzhou District, is located in the middle of the Dong River and has recently attracted considerable attention because of emerging eutrophication (Qiu et al. 2016).

Using the digital elevation model (DEM) to extract the sub-river basin (ArcMap 10.6, Esri, Inc.), we divided our study area into three sub-reaches (Fig. 1). From the upper to the lower reach, due to the topography and the coastal conditions, the area of building land is constantly increasing, whereas those of forests and shrubland are decreasing. The area of arable land remains relatively stable (Fig. 1d).

The average temperature of the study area ranges from 17 to 21 °C, with an average annual precipitation from 1010 to

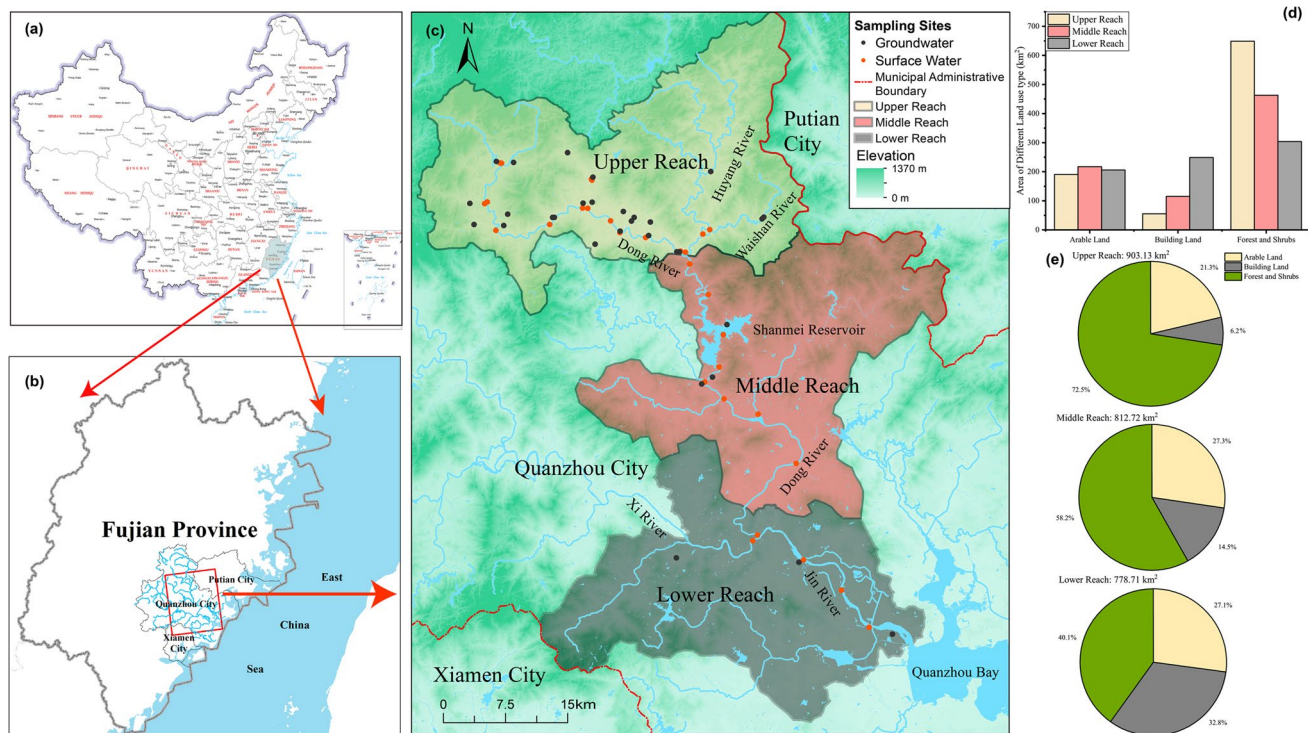


**Fig. 1** a–c Location of the study area. **d, e** Statistics of different land use types of 2020 in the study area. The land use map of the study area is included in the Supplemental Material (Fig. S1), obtained from the Chinese Global30 project (Jun et al. 2014)

1756 mm, of which 70% fall between June and September. Electronic, textile, and paper industries are widely distributed along the Jin River Basin (Li et al. 2022), and decades of rapid economic growth have resulted in significant increases in activities related to anthropogenic N, such as population growth, sewage discharge, and the extensive application of chemical fertilizers (Yu et al. 2015). In addition, the construction of large-scale water conservancy facilities, such as Shanmei Reservoir, combined with the temporally uneven distribution of flow rate and spatially different land use types, may greatly alter the nitrogen transformation in our study area (Cao et al. 2014; Wu et al. 2017).

### Sampling design

Samples were collected in June 2020 (high-flow period) and November 2020 (low-flow period) along the Jin River. During each cruise, 30 surface water samples (17, 8, and 5 for upper reach, middle reach, and lower reach, respectively) and 30 groundwater samples (24, 3, and 3 from upper to lower sub-reach) were collected (Fig. 1). The sampling sites are described in more detail in the Supplemental Material (Table S1).

Surface water samples were collected using organic glass hydrophores, and groundwater samples were taken with a peristaltic pump. For each sample, dissolved oxygen (DO), electrical conductivity (EC), total dissolved solid (TDS), oxidation–reduction potential (ORP), and pH were measured in situ (Manta + 3.0, Eureka, USA), along with turbidity (2100Q, Hach, USA). Samples were collected in 100-mL acid-washed polyethylene bottles for the analysis of isotope composition ( $\delta^{15}\text{N-NO}_3^-$ ,  $\delta^{18}\text{O-NO}_3^-$ ,  $\delta\text{D-H}_2\text{O}$ , and  $\delta^{18}\text{O-H}_2\text{O}$ ); in addition, 1-L samples were collected for the analysis of the main ion concentrations. For the surface water, another 500-mL sample was collected from each site, and 0.2 mL saturated  $\text{HgCl}_2$  was added to inhibit bacterial activity; these samples were used for the analysis of total organic carbon (TOC) and total dissolved nitrogen (TDN) and for the extraction of chlorophyll *a* (Chl-*a*). All samples were stored in an incubator at 4 °C and transported to the laboratory within 4–6 h.

### Hydrochemical and stable isotope analysis

Samples for ion concentration measurement were first filtered through a 0.45- $\mu\text{m}$  cellulose acetate filter, and subsequently, the concentrations of anions ( $\text{Cl}^-$ ,  $\text{NO}_3^-$ ,  $\text{NO}_2^-$ ,  $\text{SO}_4^{2-}$ ) were determined using a spectrophotometer (PerkinElmer Lambda 35, USA) with a precision of 5%. The analysis of cations ( $\text{Na}^+$ ,  $\text{K}^+$ ,  $\text{Ca}^{2+}$ ,  $\text{Mg}^{2+}$ ) in the water samples was performed via an inductively coupled plasma mass spectrometer (7500 ICP-MS, Agilent, USA), and  $\text{NH}_4^+$  was analyzed by Nessler's reagent spectrophotometric methods

(UV2600, Shimadzu, Japan). Total alkalinity (as  $\text{HCO}_3^-$ ) was determined by titration with standard 0.1 N hydrochloric acid, using methyl orange and phenolphthalein as indicators, with a precision of  $\pm 5\%$ .

The TOC was measured using a total organic analyzer (TOC-V, Shimadzu, Japan). After filtering through a 0.45- $\mu\text{m}$  cellulose acetate filter, the TDN of the water samples was determined using persulfate digestion and a UV spectrophotometer (UV2600, Shimadzu, Japan). The Chl-*a* was extracted with acetone (90%) (V/V) in the dark for 24 h after filtering through 0.7- $\mu\text{m}$  GF/F glass filters, followed by analysis using a spectrophotometer (UV2600, Shimadzu, Japan) as described elsewhere (Yang et al. 2017).

Both  $\delta^{15}\text{N-NO}_3^-$  and  $\delta^{18}\text{O-NO}_3^-$  were determined via the denitrified method (Sigman et al. 2001; Yi et al. 2017). Specifically, the denitrifying bacterium *Pseudomonas aureofaciens* convert nitrate to nitrous oxide, which is then concentrated and purified in a Tracegas system, and the composition is determined using an isotope ratio mass spectrometer (IsoPrime100, IsoPrime, Germany). For analysis of  $\text{H}_2\text{O}$  stable isotopes, the  $\delta^{18}\text{O}$  value was determined using  $\text{CO}_2\text{-H}_2\text{O}$  equilibration mass spectrometry, whereas the  $\delta\text{D}$  value was determined using  $\text{H}_2\text{-H}_2\text{O}$  equilibration mass spectrometry under the catalysis of platinum (Wang et al. 2020), followed by analysis with a gas isotope mass spectrometer (MAT 253, Thermo Fisher, USA). The stable isotopic ratio values are reported in parts per thousand (‰) relative to atmospheric  $\text{N}_2$  for  $\delta^{15}\text{N}$  and Vienna Standard Mean Ocean Water (VSMOW) for  $\delta\text{D}$  and  $\delta^{18}\text{O}$  (Eq. 1)

$$\delta_{\text{sample}} = (R_{\text{sample}}/R_{\text{standard}} - 1) \times 1000\text{‰} \quad (1)$$

### Multivariate statistical techniques

The homogeneity of variances and the normality of the residuals of each variable was first analyzed using the Kolmogorov–Smirnov test. If the above assumptions were both met, the differences of the variables among the groups (samples collected in different sampling periods and different sub-reach reaches) were compared using two-way ANOVA, or Student's *t* test and one-way ANOVA when only one classification variable was considered (i.e., different samplings periods, whether sample type is groundwater or surface water, and different sub-reaches of sampling sites).

If the data failed to meet the above assumptions, the non-parametric Kruskal–Wallis test or the Mann–Whitney *U* test was applied to compare the data among different reaches and sampling periods (Torres-Martínez et al. 2021). Differences were considered to be significant if  $p < 0.05$ . Linear regression analysis and Spearman correlation were applied to determine the relationship between major ions or the isotopic ratio values (Cao et al. 2021).



## Estimation of potential nitrogen sources

### Estimation based on Bayesian mixing model analysis

After the quantification of  $\delta^{15}\text{N}-\text{NO}_3^-$  and  $\delta^{18}\text{O}-\text{NO}_3^-$ , the measured data were used as input (customer) for MixSIAR, a Bayesian mixing model which can evaluate the contribution of different nitrate sources to the collected water samples (Parnell et al. 2013; Stock et al. 2014). Atmospheric deposition (AD), synthetic fertilizer (SF, mainly  $\text{NH}_4^+$  fertilizer in our study), sewage and manure (S&M), and soil nitrogen (SN) were used as four potential nitrate sources. The nitrate fertilizer was not considered as a main nitrate source in our study area, because both field survey and the published papers indicate that the most commonly used nitrogen fertilizers in China are urea and ammonium carbonate (Yang et al. 2013; Ding et al. 2015; Zhang et al. 2018). Furthermore, the main form of nitrate contained inorganic fertilizer is ammonium nitrate ( $\text{NH}_4\text{NO}_3$ ), which also contains ammonium. The distribution of nitrate isotope composition also verified that  $\text{NO}_3^-$  fertilizer (Fig. 3) was not likely to be a main source of nitrate in our study area, for there were few samples close to the edge of  $\text{NO}_3^-$  fertilizer boundary.

The detailed equations and parameter settings of MixSIAR, as well as the ranges of the isotopic ratios for potential nitrate sources are provided in the Supplemental Material (Equations S1 to S4 and Table S2). The ranges of potential sources were modified from studies in a neighboring area or studies with similar hydrologic and land use patterns (Li et al. 2018; Guo et al. 2020).

### Estimation of the flux of potential nitrogen sources based on human activities and land use structure

To validate and address the potential limitations of the nitrogen source contribution determined by isotopic compositions and the Bayesian mixing model, we estimated the nitrogen input fluxes of different potential sources using social-economic data from the local statistical yearbook and land use data from the Chinese Global30 project (Fig. S1). Total nitrogen input was divided into point sources and non-point sources.

The calculation of nitrogen input was based on the structure of Global NEWS-DIN model (Nutrient Export from Watersheds). The calculation of nitrogen from point sources (mainly from municipal sewage) was based on the GDP purchasing power parity ( $\text{GDP}_{\text{PPP}}$ ) and urban population (Van Drecht et al. 2009).

The non-point nitrogen sources consisted of nitrogen from fertilizer, manure (from poultry raising and rural population), nitrogen fixation, and atmospheric deposition (Yan et al. 2010). The amount of urban and rural population, fertilizer application, the area of different crops, and the

livestock production volume were from statistical yearbook. Area of arable land and forest was from the land use data, and detailed information was included in the Supplemental Material (Equations S5 to S8 and Tables S3 to S5).

## Results

### Spatial-temporal variations of the nitrogen composition and hydrochemical parameters

For groundwater samples, the mean concentrations of  $\text{NO}_3^-$ -N were  $7.66 \pm 5.8 \text{ mg L}^{-1}$  and  $7.54 \pm 6.17 \text{ mg L}^{-1}$  in the high-flow period and low-flow period (expressed as mean  $\pm$  SD, Table S6), respectively. For surface water in these two periods, the values were  $1.96 \pm 1.09 \text{ mg L}^{-1}$  and  $1.52 \pm 0.96 \text{ mg L}^{-1}$ , respectively. For groundwater and surface water, there was no significant difference in nitrate concentration between the two sampling periods (two-way ANOVA:  $F(1,54) = 0.044$  [ $p = 0.835$ ] and  $F(1,54) = 1.613$  [ $p = 0.210$ ], for groundwater and surface water, respectively), and there was no significant difference for  $\text{NO}_3^-$  among different sub-reaches for surface water (two-way ANOVA:  $F(2,54) = 0.191$ ,  $p = 0.826$ ) and groundwater (two-way ANOVA:  $F(2,54) = 0.062$ ,  $p = 0.940$ ).

For surface water, nitrate was the principal component of dissolved inorganic nitrogen (DIN) and accounted for 72.77% and 59.37% of the TDN in high-flow and low-flow periods, respectively (Table S6 and Fig. S2). Regarding the TDN concentration, there was no significant difference between the two sampling periods (two-way ANOVA:  $F(1,54) = 0.167$ ,  $p = 0.685$ ), but there was a significant difference among the three reaches (two-way ANOVA:  $F(2,54) = 4.704$ ,  $p < 0.05$ ). The mean TDN concentrations of the upper, middle, and lower reaches in both periods were  $2.94 \pm 1.16 \text{ mg L}^{-1}$ ,  $2.08 \pm 0.48 \text{ mg L}^{-1}$ , and  $2.43 \pm 0.35 \text{ mg L}^{-1}$ , respectively.

The DO levels in surface and groundwater samples showed similar patterns in all three reaches, with significantly lower values in the low-flow period than in the high-flow period (two-way ANOVA:  $F(1,54) = 90.712$  [ $p < 0.05$ ] and  $F(1,54) = 138.018$  [ $p < 0.05$ ], for surface water and groundwater, respectively). For instance, the DO levels of surface water in the high-flow period were  $9.56 \pm 1.27 \text{ mg L}^{-1}$ ,  $11.05 \pm 2.69 \text{ mg L}^{-1}$ , and  $7.31 \pm 1.78 \text{ mg L}^{-1}$  for the upper, middle, and lower reaches, respectively. However, these values were only  $5.93 \pm 1.41 \text{ mg L}^{-1}$ ,  $4.73 \pm 1.56 \text{ mg L}^{-1}$ , and  $3.73 \pm 1.02 \text{ mg L}^{-1}$  in the low-flow period (Table S6). It should be noted that for surface water, the DO showed a longitudinally decreasing trend from the upper to the lower reach, irrespective of the sampling period (two-way ANOVA:  $F(2,54) = 8.252$ ,  $p < 0.05$ ), but

this pattern was not observed for groundwater (two-way ANOVA:  $F(2,54) = 1.850, p = 0.167$ ).

The pH variation was similar to that of DO ( $r = 0.88, p < 0.001$ , Fig. S7); the pH was always significantly higher in the high-flow period for both surface water and groundwater in all reaches (two-way ANOVA:  $F(1,54) = 94.844 [p < 0.05]$  and  $F(1,54) = 258.421 [p < 0.05]$ , for surface water and groundwater, respectively). Irrespective of samples type (i.e., surface water or groundwater), the pH was  $8.01 \pm 0.36, 8.22 \pm 0.69$ , and  $7.85 \pm 0.36$  from the upper reach to the lower reach in the high-flow period and significantly decreased to  $6.40 \pm 0.46, 6.29 \pm 0.58$ , and  $6.80 \pm 0.38$  in the low-flow period (Table S7; two-way ANOVA:  $F(1,114) = 212.366, p < 0.05$ ).

Chloride is a widely acknowledged conservative chemical tracer. The concentration of chloride in surface water did not significantly differ among the three reaches in the high-flow period (Kruskal–Wallis test,  $p = 0.136$ ), whereas in the low-flow period, the mean concentration of  $\text{Cl}^-$  in the lower reach was  $2920.54 \pm 5074.84 \text{ mg L}^{-1}$ , most likely because in the lower reach, sampling was performed at high tide when fresh water of the Jin River is mixed with seawater from Quanzhou Bay. When excluding these potentially tide-influencing samples, the concentration of  $\text{Cl}^-$  was still significantly higher in the low-flow period compared to that in the high-flow period (Student's  $t$  test,  $p < 0.05$ ). For groundwater, there was no significant difference between the two sampling periods (Student's  $t$  test,  $p = 0.63$ ), and the  $\text{Cl}^-$  concentration of groundwater in the lower reach was  $33.78 \pm 10.29 \text{ mg L}^{-1}$ , which was significantly larger than in the upper two reaches (one-way ANOVA:  $F(2,59) = 18.392, p < 0.05$ ).

### Spatial–temporal variations in water and nitrate isotope composition

Despite of sample type (groundwater or surface water),  $\delta^{15}\text{N-NO}_3^-$  was generally heavier in the low-flow period ( $5.68\text{‰} \pm 2.11\text{‰}$ , Table S7) than in the high-flow period ( $5.06\text{‰} \pm 4.92\text{‰}$ , Mann–Whitney  $U$  test,  $p < 0.04$ ). As shown in Fig. 2,  $\delta^{15}\text{N-NO}_3^-$  of surface water was not significantly different between the two sampling periods ( $6.75\text{‰} \pm 4.77\text{‰}$  in the high-flow period and  $5.62\text{‰} \pm 2.18\text{‰}$  in the low-flow period, Mann–Whitney  $U$  test,  $p = 0.95$ ); however,  $\delta^{15}\text{N-NO}_3^-$  of groundwater in the low-flow period ( $5.75\text{‰} \pm 2.08\text{‰}$ ) was significantly heavier than that in the high-flow period ( $3.37\text{‰} \pm 4.54\text{‰}$ , Mann–Whitney  $U$  test,  $p < 0.05$ ).

For all water samples in two sampling periods,  $\delta^{18}\text{O-NO}_3^-$  was significantly heavier in the low-flow period ( $10.11\text{‰} \pm 3.79\text{‰}$ ) than in the high-flow period ( $0.19\text{‰} \pm 5.93\text{‰}$ , Mann–Whitney  $U$  test,  $p < 0.05$ ). In the high-flow period,  $\delta^{18}\text{O-NO}_3^-$  did not significantly differ between surface water ( $1.38\text{‰} \pm 4.09\text{‰}$ ) and groundwater ( $-1.01\text{‰} \pm 7.21\text{‰}$ , Mann–Whitney  $U$  test,  $p = 0.28$ ), but the  $\delta^{15}\text{N-NO}_3^-$  in surface water was higher than that in groundwater (Student's  $t$  test,  $p < 0.05$ ). In the low-flow period, the opposite pattern was observed;  $\delta^{15}\text{N-NO}_3^-$  did not significantly differ between surface water and groundwater (Student's  $t$  test,  $p = 0.81$ ), but the mean  $\delta^{18}\text{O-NO}_3^-$  of surface water was  $11.48\text{‰} \pm 4.09\text{‰}$ , which was significantly heavier than that of groundwater ( $8.73\text{‰} \pm 2.93\text{‰}$ , Student's  $t$  test,  $p < 0.05$ ).

Evaporation was anticipated due to the high temperatures ( $22\text{--}29 \text{ }^\circ\text{C}$ ) throughout the study period. However, there were no significant differences observed in both

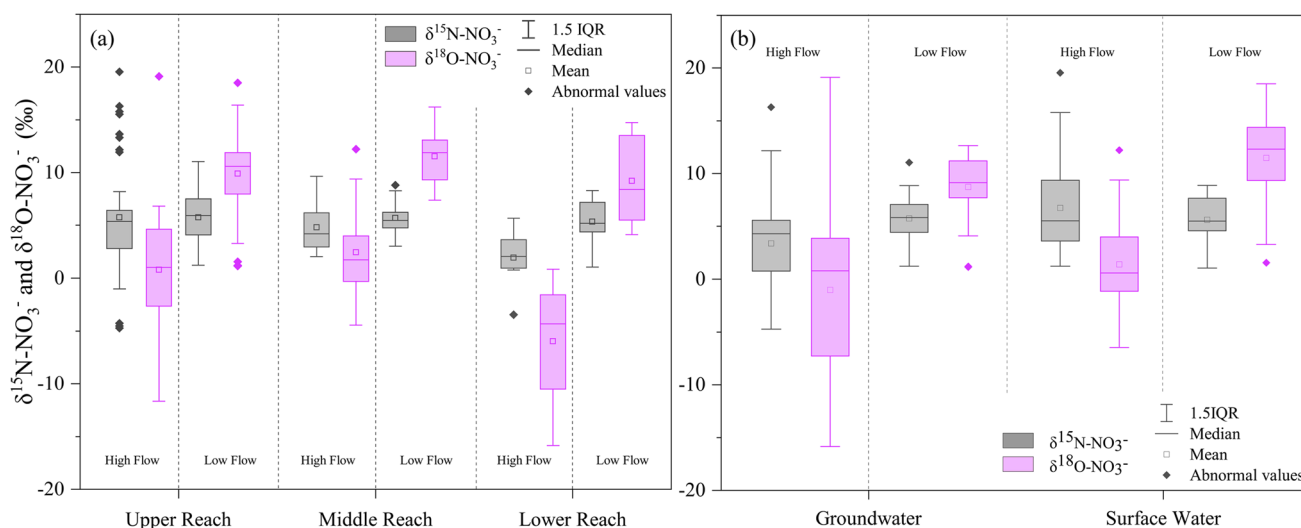


**Fig. 2** Box plots of nitrate stable isotope ratio. **a** Ratio for samples from different reaches in the two sampling periods. **b** Ratio for samples of groundwater and surface water in the two sampling periods

$\delta\text{D-H}_2\text{O}$  and  $\delta^{18}\text{O-H}_2\text{O}$  isotope values between the two sampling periods (two-way ANOVA:  $F(1,114) = 1.726$  [ $p = 0.19$ ] and  $F(1,114) = 2.835$  [ $p = 0.095$ ] for  $\delta\text{D-H}_2\text{O}$  and  $\delta^{18}\text{O-H}_2\text{O}$ , respectively). In contrast, during the low flow period, these two isotopes were significantly heavier in the lower reach (two-way ANOVA:  $F(2,114) = 9.548$  [ $p < 0.05$ ] and  $F(2,114) = 9.286$  [ $p < 0.05$ ] for  $\delta\text{D-H}_2\text{O}$  and  $\delta^{18}\text{O-H}_2\text{O}$ , respectively), suggesting a greater evaporation closer to the estuary, which could be expected due to the absence of shade and the low water movement, in contrast to the upstream sites with high tree cover and fast-moving water (Erostate et al. 2018; Cao et al. 2020). The potential effects of the above factors on the isotopic compositions of water could be probably more evident in the low flow period.

Different nitrate sources have specific stable isotope ratios (Soto et al. 2019; Guo et al. 2021). According to Fig. 3, most samples were within the intersecting area of synthetic fertilizer ( $\text{NH}_4^+$  fertilizer), soil nitrogen, and sewage and manure, whereas no samples fell into the typical range of atmospheric deposition and  $\text{NO}_3^-$  fertilizer. However, the isotope compositions of natural water samples had been altered due to fractionation and mixing effects among different sources.

Theoretically, if nitrification occurs and plays an important role in nitrate transformation,  $\delta^{18}\text{O-H}_2\text{O}$  could be calculated according to Eq. 2. As the result of  $\delta^{18}\text{O-O}_2$  being assumed to be 23.5‰ (Du et al. 2017) and the  $\delta^{18}\text{O-H}_2\text{O}$  in our study area ranging between  $-7.5$  and  $2.5$ ‰, the

potential range of  $\delta^{18}\text{O-NO}_3^-$  is also shown in Fig. 3. It can be assumed that nitrification was more likely to occur in the high-flow period.

The slopes of  $\delta^{18}\text{O-NO}_3^-$  versus  $\delta^{15}\text{N-NO}_3^-$  were 0.88 ( $r = 0.48$ ,  $p < 0.001$ , Figs. 3 and S7) and 0.86 ( $r = 0.72$ ,  $p < 0.001$ , Figs. 3 and S8) for samples in both sampling periods and high-flow period, respectively. Both slopes were within the range of the isotope enrichment factor caused by denitrification (Archana et al. 2018). However, in the low-flow period, there was no significant relationship between  $\delta^{18}\text{O-NO}_3^-$  and  $\delta^{15}\text{N-NO}_3^-$  ( $r = 0.20$ ,  $p > 0.05$ , Fig. S9, fitting line is not shown in Fig. 3), indicating that nitrate transformation in the low-flow period was somewhat more sophisticated, and mixing effects among different processes and sources are common.

$$\delta^{18}\text{O-NO}_3^- = \frac{1}{3} \delta^{18}\text{O-O}_2 + \frac{2}{3} \delta^{18}\text{O-H}_2\text{O} \quad (2)$$

### Proportional contribution of different nitrogen sources

#### Source apportionment based on the MixSIAR

According to the anthropogenic activities in the study area and the results in Fig. 3, AD, S&M, SF, and SN are the four potential nitrate sources. The results obtained from MixSIAR showed that in the high-flow period, SF was the main nitrate source for all sub-reaches (Fig. S10 and Table 1), and

**Fig. 3** Variations of  $\delta^{15}\text{N-NO}_3^-$  versus  $\delta^{18}\text{O-NO}_3^-$  values in water samples of the Jin River Basin from two sampling periods. The ranges of the typical isotopic compositions of different nitrate sources were referenced according to previous studies (Kendall et al. 2000; Han and Currell 2022): ①  $\text{NO}_3^-$  fertilizer, ②  $\text{NH}_4^+$  fertilizer, ③ sewage and manure, ④ soil nitrogen, and ⑤ atmospheric deposition

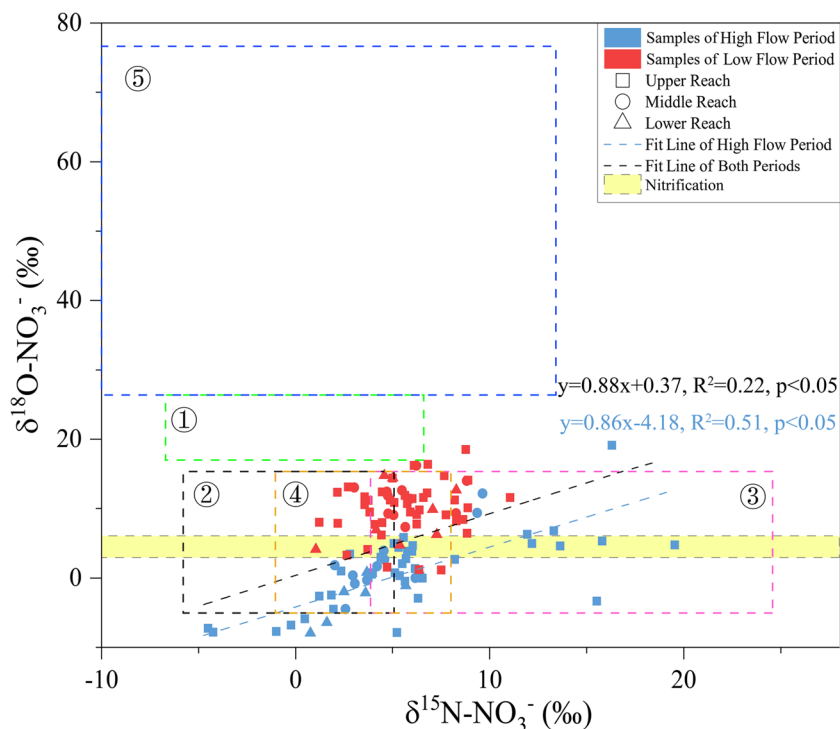


**Table 1** Contributions of four potential nitrate sources calculated by MixSIAR for different sub-reaches of the Jin River Basin in two sampling periods

Period	Reach	Sources (mean $\pm$ SD)			
		Atmospheric deposition	Sewage and manure	Soil nitrogen	Synthetic fertilizer
High flow	Upper reach	11.6 $\pm$ 1.3	8.2 $\pm$ 3.9	37.3 $\pm$ 6.5	42.8 $\pm$ 6.3
	Middle reach	13.9 $\pm$ 2.4	9.7 $\pm$ 5.1	26 $\pm$ 7.3	50.4 $\pm$ 9.5
	Lower reach	7.5 $\pm$ 1.6	3.5 $\pm$ 2.5	28 $\pm$ 7.2	60.9 $\pm$ 8.1
	All reaches	11 $\pm$ 1.8	7.1 $\pm$ 3.8	30.4 $\pm$ 7	51.4 $\pm$ 8
Low flow	Upper reach	28.9 $\pm$ 1.5	33.3 $\pm$ 4.8	18.9 $\pm$ 4.2	18.9 $\pm$ 5.1
	Middle reach	31.7 $\pm$ 2.6	35.6 $\pm$ 5.5	12.1 $\pm$ 3.7	20.6 $\pm$ 6.2
	Lower reach	25.3 $\pm$ 3.2	18.8 $\pm$ 8	19.3 $\pm$ 5.7	36.6 $\pm$ 9
	All reaches	28.6 $\pm$ 2.4	29.2 $\pm$ 6.1	16.8 $\pm$ 4.5	25.4 $\pm$ 6.8
Both periods	Upper reach	20.3 $\pm$ 1.4	20.8 $\pm$ 4.4	28.1 $\pm$ 5.4	30.9 $\pm$ 5.7
	Middle reach	22.8 $\pm$ 2.5	22.7 $\pm$ 5.3	19.1 $\pm$ 5.5	35.5 $\pm$ 7.9
	Lower reach	16.4 $\pm$ 2.4	11.2 $\pm$ 5.3	23.7 $\pm$ 6.5	48.8 $\pm$ 8.6
	All reaches	19.8 $\pm$ 2.1	18.2 $\pm$ 5	23.6 $\pm$ 5.8	38.4 $\pm$ 7.4

the contribution of these sources longitudinally increased from the upper reach (42.8%  $\pm$  6.3%) to the lower reach (60.9%  $\pm$  8.1%). Furthermore, SN and AD were the second and third nitrate sources, respectively, whereas S&M was the least significant nitrate source, and its contribution decreased from the upper to the lower section. In the lower reach, it only accounted for 3.5%  $\pm$  2.5%, which was somewhat unexpected, especially in a highly urbanized coastal river basin.

In the low-flow period, for all three sub-reaches, the different sources followed the order S&M (29.2%  $\pm$  6.1%), AD (28.6%  $\pm$  2.4%), SF (25.4%  $\pm$  6.8%), and SN (16.8%  $\pm$  4.5%). The mean contribution of the above potential nitrate sources was significantly different from the findings in the high-flow period, in which the contribution of AD and S&M was significantly higher in the low-flow period than in the high-flow period (two-way ANOVA:  $F(1,16) = 10.817$  [ $p < 0.05$ ] and  $F(1,16) = 16.991$  [ $p < 0.05$ ] for AD and S&M, respectively), but SN and SF were opposite to this result (two-way ANOVA:  $F(1,16) = 6.498$  [ $p < 0.05$ ] and  $F(1,16) = 23.518$  [ $p < 0.05$ ] for SN and SF, respectively). In the lower reach, it was 36.6%, almost twice as high as that in the upper reach (18.9%  $\pm$  5.1%). Although the contribution of SF varied significantly between the two sampling periods, the spatial variation of the contribution from SF remained stable for both sampling periods (Kruskal–Wallis test,  $p > 0.05$ ; Table 1 and Table S8).

#### Source apportionment based on the estimation of the flux of potential nitrogen sources

The contributions of various nitrogen sources, as estimated by the Global NEWS-DIN model equations (Equations S5 to S8), are presented in Fig. 4. It is important to note that the basic social-economic data used in this analysis were obtained from the most recently published local statistics

yearbook and therefore reported on an annual rather than quarterly basis. This limitation made it difficult to apportion the nitrogen input of each source to different sampling periods.

The results depicted in Fig. 4 indicate that synthetic fertilizer was the principal nitrogen source for the upper reach (69.66%) and the second most significant source for the middle (23.25%) and lower (26.10%) reaches. The combined contribution of nitrogen from sewage and manure increased gradually from the upper to lower reaches. Nitrogen deposition (both wet and dry deposition) was the third most significant nitrogen source in our study area, while nitrogen fixed by crops and forest accounted for only about 1% of the total nitrogen input.

While similarities existed between the results of source estimation using MixSIAR and the calculations of various nitrogen input fluxes (Global NEWS-DIN model), it became evident that there were discrepancies and even contradictions in the determination of certain sources when comparing the estimated results of MixSIAR and the different nitrogen source input fluxes, particularly for the contributions of SF and S&M. The possible causes of this discrepancy are discussed further in sections “[Comparison of the contribution obtained by MixSIAR and calculation of nitrogen source fluxes](#)” and “[Limitation of the approach.](#)”

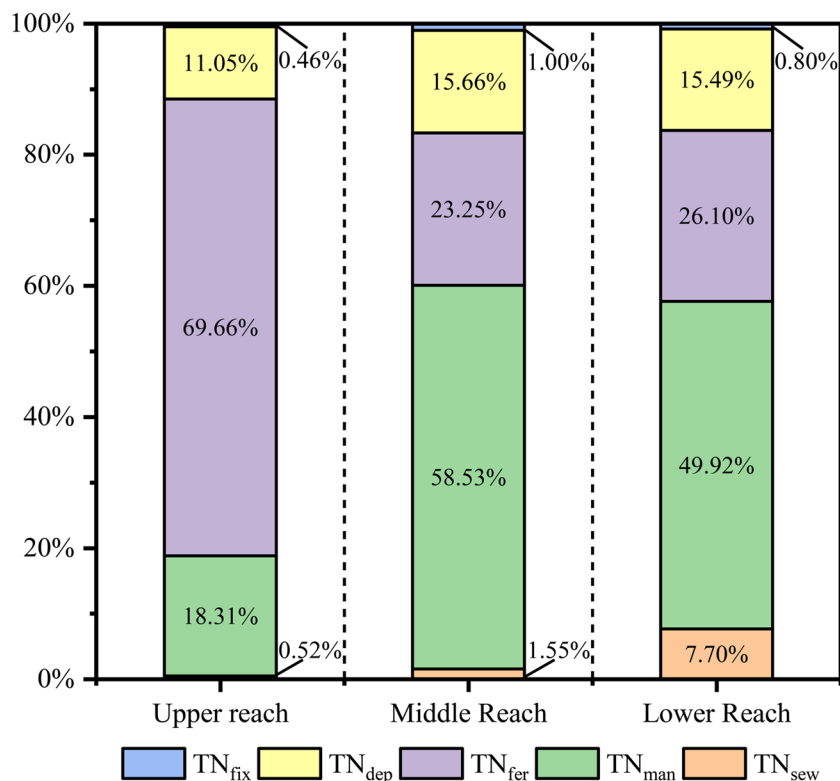
## Discussion

### Characteristics of nitrate transformation in both sampling periods

Although chlorophyll *a* can serve as a proxy of phytoplankton biomass, for the two sampling periods, the concentration of Chl-*a* did not vary significantly (Student’s *t* test,



**Fig. 4** Percent contribution of different nitrogen sources estimated by local social-economic data



$p = 0.348$ ). However, the mean TOC concentration in the high-flow period was  $5.74 \text{ mg L}^{-1}$  (Table S7), which was significantly higher than that in the low-flow period (Student's  $t$  test,  $p < 0.05$ ). This leads us to infer that the quantity of microorganisms in the two sampling periods had the same order of magnitude, but the microbial activities were probably more active in the high-flow period.

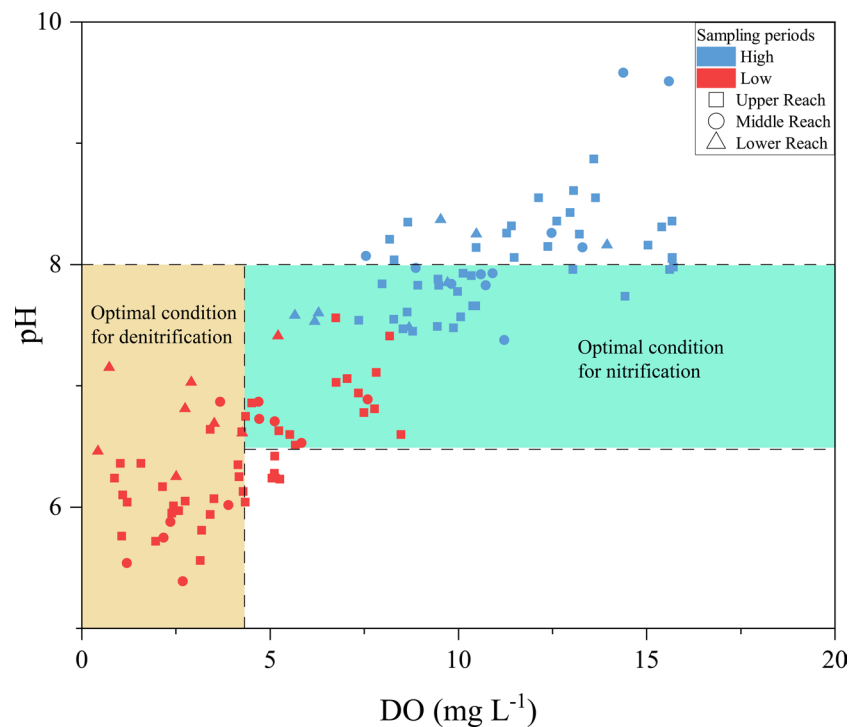
The isotopic composition of  $\text{NO}_3^-$  is not only useful for source identification but can also be applied to investigate the influences of nitrification and denitrification. Considering the depletion of  $\delta^{18}\text{O-NO}_3^-$  in the high-flow period (Fig. 3), it could be inferred that nitrification was more pronounced in summer, probably because of the higher temperatures. On the other hand, the wider distribution of  $\delta^{15}\text{N-NO}_3^-$  in the high-flow period also suggests the occurrence of nitrate assimilation. Algae/biota preferentially take up light isotopes of  $\text{NO}_3^-$ , which would lead to enrichment with heavy isotopes in residual  $\text{NO}_3^-$  (Casciotti 2016). The ratio of  $\delta^{18}\text{O-NO}_3^-$  to  $\delta^{15}\text{N-NO}_3^-$  was 0.86 in the high-flow period (Fig. 3), close to the 1:1 increase reported for  $\text{NO}_3^-$  assimilation of marine phytoplankton (Ding et al. 2015). This ratio was also close to the reported variation caused by denitrification, which ranges from 1:1.3 to 1:2.1 between  $\delta^{18}\text{O-NO}_3^-$  and  $\delta^{15}\text{N-NO}_3^-$  (Yang et al. 2019). According to Fig. 5 and Table S7, the DO level in the high-flow period ( $11.06 \pm 2.69 \text{ mg L}^{-1}$ ) was significantly greater than that in the low-flow period ( $4.06 \pm 2.1 \text{ mg L}^{-1}$ ). High DO levels in summer can, to some extent, impede

denitrification, as this process is generally suppressed at DO levels above  $4 \text{ mg L}^{-1}$  (Cojean et al. 2019; Qiao et al. 2020).

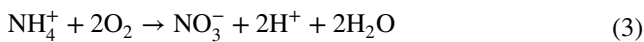
In the low-flow period, there was a significant negative relation between  $\delta^{18}\text{O-NO}_3^-$  and  $\text{NO}_3^-$  concentration ( $r = -0.31$ ,  $p < 0.05$ , Fig. S9). Combined with the significant negative correlation between pH and  $\text{NO}_3^-$  concentration ( $r = -0.41$ ,  $p < 0.01$ , Fig. S9), nitrification may also occur in the low-flow period, which might have caused the elevated  $\text{NO}_3^-$  concentration with decreasing pH, according to Eq. 3 (Kim et al. 2015). The higher  $\delta^{18}\text{O-NO}_3^-$  in the low-flow period indicates the impact of nitrate from atmospheric deposition, which greatly enhanced  $\delta^{18}\text{O-NO}_3^-$  in winter; this hypothesis was supported by the results of the MixSIAR (Table 1).

From the high- to the low-flow period, with the slight enrichment of  $\delta^{15}\text{N-NO}_3^-$  from  $5.06\text{‰} \pm 4.92\text{‰}$  to  $5.68\text{‰} \pm 2.11\text{‰}$  and the significant enrichment of  $\delta^{18}\text{O-NO}_3^-$  from  $0.19\text{‰} \pm 5.93\text{‰}$  to  $10.11\text{‰} \pm 3.79\text{‰}$  (Mann–Whitney  $U$  test,  $p < 0.05$ ), denitrification may also occur in the low-flow period. Although DO was significantly lower in the low-flow period ( $4.06 \pm 2.1 \text{ mg L}^{-1}$ ) than in the high-flow period ( $11.06 \pm 2.69 \text{ mg L}^{-1}$ , mentioned in the section “Spatial–temporal variations of the nitrogen composition and hydrochemical parameters”), this value in the low-flow period was neither low enough to impede nitrification nor high enough to impede denitrification (Cojean et al. 2019; Li et al. 2023), indicating the limited co-occurring of nitrification and denitrification in the low-flow period. Considering that TOC was lower in the low-flow period and there was no significant

**Fig. 5** Scatterplot contrasting pH with DO, where the parts divided by dashed lines represent the suitable conditions for nitrification (right side) and denitrification (left side), as described previously (Torres-Martínez et al. 2021)



relationship between  $\delta^{18}\text{O}\text{-NO}_3^-$  and  $\delta^{15}\text{N}\text{-NO}_3^-$  in the low-flow period ( $r=0.20$ ,  $p>0.05$ , Fig. S9), it is reasonable to hypothesize that the mixing effect of different sources was the main factor influencing nitrate transformation in the low-flow period and thus somehow masked the occurrence of nitrification and denitrification.



### Relationships between nitrate sources and hydrochemical parameters in different sub-reaches

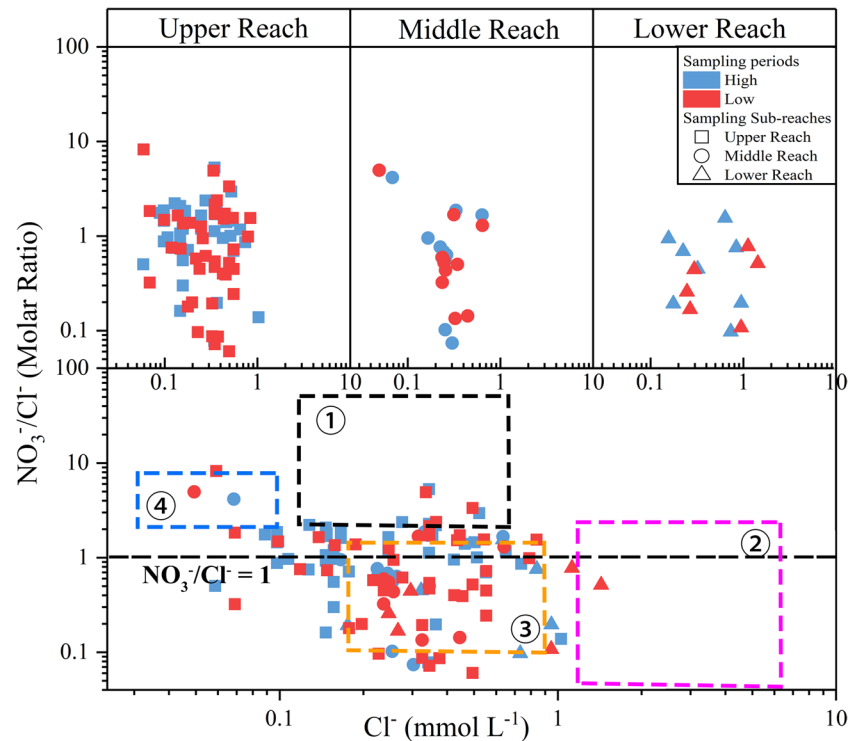
The stable nitrate isotopic compositions of the samples from the different sub-reaches did not vary significantly in the low-flow period (one-way ANOVA:  $F(2,57)=0.114$  [ $p=0.892$ ] and  $F(2,57)=1.073$  [ $p=0.349$ ] for  $\delta^{15}\text{N}\text{-NO}_3^-$  and  $\delta^{18}\text{O}\text{-NO}_3^-$ , respectively). In the high-flow period, although  $\delta^{15}\text{N}\text{-NO}_3^-$  still showed a similar distribution in all three sub-reaches (one-way ANOVA:  $F(2,57)=2.087$ ,  $p=0.133$ ), however, the  $\delta^{18}\text{O}\text{-NO}_3^-$  of samples in the lower reach ( $-5.97\text{‰} \pm 6.00\text{‰}$ ) was significantly lower than that in the other two reaches (two-way ANOVA:  $F(2,114)=8.449$ ,  $p<0.05$ ; Fig. S11), suggesting that for the lower reach, nitrification was the dominant nitrate transformation process in summer, causing the downstream depletion of  $\delta^{18}\text{O}\text{-NO}_3^-$ .

For the upper and the middle reaches, there was a significant positive correlation between  $\delta^{18}\text{O}\text{-NO}_3^-$  and

$\delta^{15}\text{N}\text{-NO}_3^-$  in the high-flow period ( $r=0.71$  and  $0.86$ ,  $p<0.01$ ; Figs. S3 and S4). As discussed above, denitrification was unlikely to play an important role in the high-flow period, and therefore, this phenomenon suggests that high nitrogen input from synthetic fertilizer had successively stimulated the nitrification of  $\text{NH}_4^+$  and nitrate assimilation, resulting in  $\delta^{18}\text{O}\text{-NO}_3^-$  and  $\delta^{15}\text{N}\text{-NO}_3^-$  enrichment. Furthermore, due to the significant impact of synthetic fertilizer,  $\text{NH}_4^+$  volatilization and remineralization also occurred (Minet et al. 2017; Spalding et al. 2018), which is in accordance with the high contribution of nitrate from SF and SN for the upper reach in the high-flow period.

It should be noted that for samples from the lower reach, there was no significant correlation between  $\delta^{15}\text{N}\text{-NO}_3^-$  and  $\ln(\text{NO}_3^-)$  (statistics shown in Fig. S5). With the increase in  $\ln(\text{NO}_3^-)$ ,  $\delta^{15}\text{N}\text{-NO}_3^-$  almost remained constant. However, there was a negative correlation between  $\delta^{18}\text{O}\text{-NO}_3^-$  and  $\ln(\text{NO}_3^-)$  in lower reach, especially during the low-flow period, although this relation was insignificant (statistics shown in Fig. S6). This leads us to infer that for the lower reach, continued input from a single source of nitrate has led to increasing nitrate concentrations, while the isotope composition remained largely stable because of the unchanged nitrate sources (Cao et al. 2015). However, nitrification may have a certain influence on the depletion of  $\delta^{18}\text{O}\text{-NO}_3^-$  and the decrease in the  $\text{NO}_3^-$  concentration. In the low-flow period, the enhanced denitrification

**Fig. 6**  $\text{Cl}^-$  molar concentrations with  $\text{NO}_3^-/\text{Cl}^-$  molar ratios of water samples collected in both sampling periods from different sub-reaches of the Jin River Basin. From ① to ④ are the typical ranges of  $\text{NO}_3^-/\text{Cl}^-$  molar ratios and  $\text{Cl}^-$  concentration from synthetic fertilizer, sewage and manure, soil nitrogen, and atmospheric decomposition, based on the published studies (Ogrinc et al. 2019; Li et al. 2023)



due to the lower DO and the higher nitrate level also caused the negative correlation between  $\delta^{18}\text{O}-\text{NO}_3^-$  and  $\text{NO}_3^-$  concentration ( $r = -0.74$ ,  $p < 0.05$ , Fig. S9).

Most samples in Fig. 6 fell within the ranges of soil nitrogen. According to the results of different N source flux calculations (Fig. 5), the annual nitrogen fixed by crops and forests only accounted for about 1% of the total nitrogen input. Therefore, natural nitrogen fixation cannot explain why soil nitrogen had such a strong impact on the source of nitrogen. Soil nitrogen may represent the nitrogen from other main sources, fixed by the bacteria in the soil and the vadose zone via the nitrogen assimilation process.

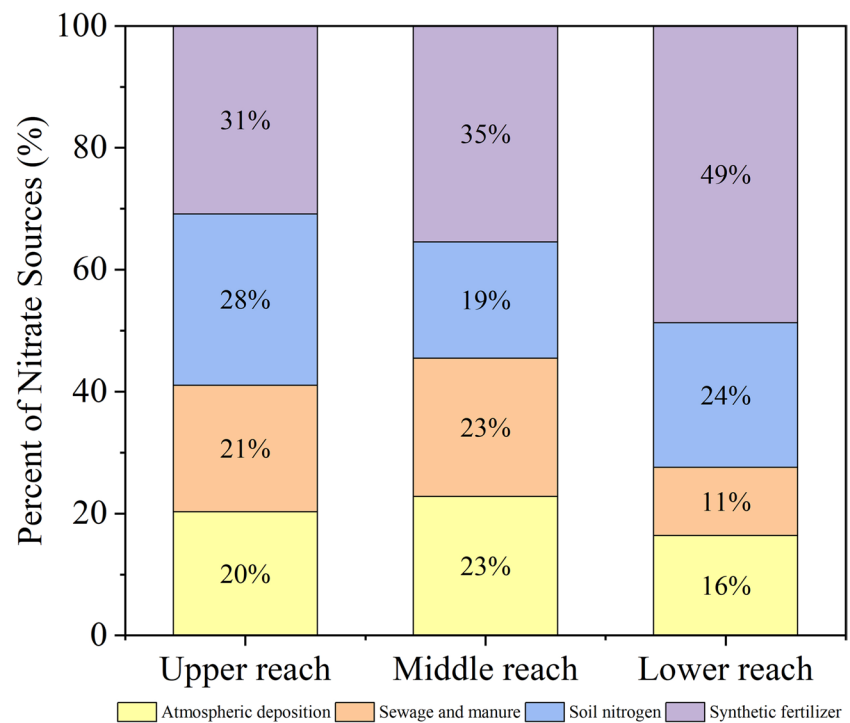
SF and S&M were the two main nitrogen sources observed in both MixSIAR and nitrogen source flux calculations, suggesting the mixing of different nitrate sources. Although the distribution of  $\text{NO}_3^-$  versus  $\text{Cl}^-$  molar ratio of most samples was around 0.4, considering the average of this value was about 1.12 and the large nitrogen input fluxes of SF (Fig. 4), it was reasonable to hypothesize that samples from the upper two reaches were strongly impacted by SF (Fig. 6), which has a relatively higher  $\text{NO}_3^-/\text{Cl}^-$  molar ratio with a low  $\text{Cl}^-$  concentration (Li et al. 2018; Ren et al. 2022). Therefore, the relationship between  $\text{NO}_3^-/\text{Cl}^-$  molar ratio and  $\text{Cl}^-$  also verified the nitrate sources and transformation processes were strongly influenced by non-point agricultural sources (Torres-Martínez et al. 2021).

### Comparison of the contribution obtained by MixSIAR and calculation of nitrogen source fluxes

By comparing Fig. 7 and Fig. 4, the comparison between the results estimated by the concentration-based approach (MixSIAR) and the flux-based approach (Global NEWS-DIN model) revealed some discrepancies. Compared to the Global NEWS-based estimates, MixSIAR seemed to underestimate the nitrogen contribution from S&M in the middle and lower reaches, and it underestimated the nitrogen contribution from SF in the upper reach but overestimates it in the other two reaches. These phenomena indicate that the calculation of fluxes can aid in distinguishing the contributions of manure and sewage. Additionally, the discrepancies in the contribution of SF estimated by the two methods highlight the substantial influence of hydraulic connectivity. Non-point source pollution can result in significant degradation of the water environment, even in the middle and lower areas of a coastal watershed.

The discrepancies between the two methods can be attributed to two factors. Firstly, as mentioned in the section “Source apportionment based on the estimation of the flux of potential nitrogen sources,” the social-economic data used in the calculation of nitrogen fluxes were annual and could not be broken down into specific months, whereas the input data for MixSIAR were based on two sampling periods. Nitrogen sources and their contribution are constantly changing throughout the year, and this could lead to differences in the

**Fig. 7** Mean contributions of four nitrate sources in the Jin River Basin for the three different reaches estimated by MixSIAR (irrespective of sampling periods)



estimated results between the two methods (shown in the section “[Source apportionment based on the MixSIAR](#)”).

Secondly, due to the limitation of data availability, we could only estimate the total nitrogen from different sources and calculate the respective percent contribution of each nitrogen source. In other words, this treatment is somewhat equivalent to treating each sub-reach as a closed/static system and ignoring the transport and transformation of nitrogen driven by the hydrological cycle.

Despite the aforementioned limitations in the calculation of nitrogen source fluxes, comparing this method with the Bayesian mixing model precisely reflects the importance of the ecosystem. Estimating various nitrogen input fluxes serves as an apparent nitrogen source identification, assuming that the composition and distribution of nitrogen in the watershed remain unchanged, regardless of microbial activity in water and soil, as well as the potential impacts of surface runoff and groundwater infiltration. However, in this study, the Bayesian mixing model employed (MixSIAR) categorizes samples based on sampling period and sub-reach, examining the spatiotemporal factors that influence the major sources of nitrate. It also takes into account the mixing process of different sources and possible fractionation of isotopes caused by nitrogen transformation. Therefore, MixSIAR provides insights into the actual nitrogen sources influenced by the ecosystem. Comparing the results of both source apportionment methods can reveal the extent of human activities on the ecosystem’s capacity to mitigate nitrate pollution.

### Factors affecting nitrate contamination and transformation in coastal basins

Based on our results, the isotope composition differed significantly between the two sampling periods. Hydrological conditions and temperature could be the two main factors influencing the concentration and transformation of  $\text{NO}_3^-$  concentration, which ultimately determined the degree of nitrate contamination in both sampling periods. Although both TDN and  $\text{NO}_3^-$  concentration did not vary significantly between the sampling periods, the significant differences in TOC and temperature determined the microbial activities. Stronger nitrification causes the depletion of  $\delta^{18}\text{O}-\text{NO}_3^-$  in the high-flow period, while stronger nitrate assimilation and  $\text{NH}_4^+$  volatilization resulted in the simultaneous enrichment of  $\delta^{15}\text{N}-\text{NO}_3^-$  (Frick et al. 2022).

According to the Quanzhou Water Resource Bulletin from 2020, the average annual precipitation of the Jin River Basin was 1667 mm, of which up to 70% was concentrated in the high-flow period. Nitrate gradually accumulated from the upper to the lower reaches, most likely because of non-point source nitrate input from SF under the influence of high runoff-flushing in summer (Yi et al. 2017). This conclusion is in accordance with the results of MixSIAR and stable isotope composition, clearly showing that nitrate sources were increasingly influenced by SF from upstream to downstream. The contribution of SN was also higher in the high-flow period. According to a previous study, nitrate originates from stormwater that carries organic material, such as leaf



litter and grass clipping, from land to water in the high-flow period (Hu et al. 2019), which could explain this finding.

As mentioned earlier in the section “Proportional contribution of different nitrogen sources,” the contribution of SN was significantly higher in the high-flow period compared to the low-flow period, also suggesting the existence of legacy effects, which was caused by the transportation of nitrate from groundwater to surface water (Van Meter et al. 2018). Such a process may persist for decades, causing the elevating groundwater nitrate concentration even after the cease of N input (Weitzman et al. 2022), partly because nitrate is negatively charged and tends to be leached to groundwater because it is rejected by the also negatively charged soil particles (Cao et al. 2014). The mean nitrate concentration of groundwater was almost five times greater than that of surface water; thus, a large amount of nitrogen may leach from the aquifer (groundwater) and the soil nitrogen pool under suitable conditions (Jiang et al. 2018). Although the transportation of this leached nitrogen to surface water may take years to decades (Hamilton 2012), this process could be stimulated by high precipitation and high runoff during summer.

The high flow rate in summer could also lead to the rapid discharge of nitrate from S&M downstream. Construction land accounts for the highest proportion of all land use types in the lower reach of the Jin River Basin, and the higher runoff results in the rapid downstream transportation of nitrate from sewage. For this reason, the high contribution of S&M was somewhat masked.

According to the distribution of  $\delta^{15}\text{N-NO}_3^-$  and  $\delta^{18}\text{O-NO}_3^-$ , denitrification is unlikely to be the dominant nitrogen transformation process. The contribution of denitrification to nitrogen removal in the rainy season could be further limited due to storm flow impacts as a limited water exchange and a prolonged water residence time facilitate denitrification (Xue et al. 2014). Denitrification was enhanced in winter, most likely because of the suitable pH and DO conditions in the low-flow period. As mentioned earlier (section “Proportional contribution of different nitrogen sources”), the contribution of nitrate from AD in the low-flow period was significantly greater than that in the high-flow period. Most likely, this is the result of the weaker runoff-flushing effect caused by the lower flow rate, as nitrate from non-point contamination sources and SN are retained in the soil or vadose zone.

As discussed in sections “Spatial-temporal variations of the nitrogen composition and hydrochemical parameters” and “Relationships between nitrate sources and hydrochemical parameters in different sub-reaches,” despite the great differences in land use structure across the three sub-reaches, there appeared to be no significant variation in both  $\text{NO}_3^-$  concentration and isotope composition in the different reaches. This indicates that compared to land use structure,

hydrological and climatic conditions were the main factors influencing nitrate sources and transformation in this coastal basin. However, it should be noted that land use did have some impacts on nitrate contamination in the low-flow period as the area of construction land and the contribution of nitrate from S&M both increased downstream. Non-point source contamination from arable land, caused by the application of synthetic fertilizer, was the main cause of nitrate contamination compared to point source, such as sewage disposal. This may be particularly evident in coastal watersheds where the catchment area is relatively small and the runoff-flushing effect is strong.

### Limitation of the approach

In this study, we utilized the concentration-based approach, which combined the hydrochemical data, analysis of nitrate stable isotopes, and Bayesian mixing model during different sampling campaigns, to identify the potential sources and transformation of nitrogen under the influences of anthropogenic activities. While the data used by the concentration-based model is easier to obtain and explain, the results should be compared to those of the flux-based approach (e.g., Global NEWS-DIN model), which consider the anthropogenic activities in different sub-reaches. This is necessary to avoid misinterpreting the mixing model results as direct evidence of the importance of different inferred nitrogen sources without considering the broader context of anthropogenic activities, so as to reduce the uncertainties in source determination.

Due to the unavailability of long-term hydrology and environmental monitoring data, we calculated the input fluxes of different nitrogen sources based on annual social-economic data collected from the local statistical yearbook. However, this method did not allow for apportioning fluxes to each month or sampling period and treated each sub-reach as a closed system, ignoring the complexities of nitrogen transformation and hindering analysis of underlying mechanisms (Xu et al. 2022).

When it comes to the concentration-based approach, i.e., the Bayesian mixing model (MixSIAR), due to limitations in fieldwork time and low utilization of groundwater in some parts of our study area, obtaining a sufficient number of well samples was challenging, especially in the lower reach. As a result, the number of groundwater samples ( $n=3$ ) in the lower reach was limited, resulting in an unbalanced study design. This data deficiency should be fully considered and overcome in the design of future work. Additionally, due to limited funding, we were only able to conduct two sampling cruises in this study. Conducting quarterly sampling in 1 year would provide more comprehensive data for discussion. Although nitrate was the main form of inorganic nitrogen, the isotopic composition of other nitrogen forms

in aquatic environment, such as  $\delta^{15}\text{N-NH}_4^+$ ,  $\delta^{15}\text{N-TN}$ , and  $\delta^{15}\text{N-N}_2\text{O}$ , could greatly help reduce analysis uncertainties.

Based on the above discussion, although both the concentration-based approach (MixSIAR) and the flux-based approach (Global NEWS DIN model) used in this study have certain limitations, as mentioned in the section “Comparison of the contribution obtained by MixSIAR and calculation of nitrogen source fluxes,” the flux-based approach can reflect the “real” input intensity of different nitrogen sources. However, it falls short in capturing the spatiotemporal transformations of nitrogen composition, concentration, and sources influenced by surface runoff, groundwater infiltration, and microbial processes in water and soil. In contrast, the Bayesian mixing model (MixSIAR) incorporates categorical variables in the data structure, allowing for the consideration of temporal (sampling periods) and spatial (sub-reaches) factors on nitrogen sources. It also addresses the uncertainties in isotopic composition from various sources and accounts for fractionation effects in source apportionment. By comparing the outcomes of both methods, it is possible to assess the potential impact of human activities on nitrate pollution and the buffering capacity of the watershed ecosystem. Therefore, we recommend utilizing the mixing model as the preferred approach for identifying nitrogen sources at the watershed scale, while also cross-referencing the results with the estimation of potential nitrogen fluxes.

## Conclusions

The Jin River, which flows into Taiwan Strait, is a highly dynamic estuarine system in Southeast China. Based on our results, nitrification, nitrate assimilation by phytoplankton, and  $\text{NH}_4^+$  volatilization were the main nitrogen transformation processes in our study area, mainly because of the significant influence of nitrate from synthetic fertilizer. Although denitrification was more likely to occur in the low-flow period, its intensity was limited, and the signal of denitrification was masked by the mixing effects of different biological transformation processes and nitrate sources.

Variations in precipitation and water discharge caused different nitrate biogeochemical processes for different sampling periods and may have masked the actual nitrate sources. The contribution of synthetic fertilizer was greater in the high-flow period than in the low-flow period. For both periods, the contribution of synthetic fertilizer longitudinally increased from the upper to the lower reaches, and the contribution of nitrate from synthetic fertilizer was lower in the high-flow period. Compared to point source pollution, such as sewage disposal, synthetic fertilizer transported into the river was driven by high precipitation and runoff, which could be too rapid for specific functional microorganisms

to alleviate the excess nitrate, such as denitrifying bacteria and anammox bacteria/archaea. Thus, more efforts should be made to control non-point source pollution in the upper reaches of coastal rivers.

Our studies also highlight the importance of comparing the results obtained from both the Bayesian mixing model (MixSIAR) and the estimation of nitrogen sources (Global NEWS-DIN model). This comparison allows us to not only assess the actual intensity of nitrogen input caused by human activities but also understand the buffering effect of the watershed ecosystem, including the mitigation of nitrate pollution by the vadose zone and aquifer.

**Supplementary Information** The online version contains supplementary material available at <https://doi.org/10.1007/s11356-023-28360-9>.

**Acknowledgements** The authors would like to appreciate all the support received from local residents in sampling and measurements.

**Author contribution** Shengwei Cao: conceptualization, methodology, investigation, and writing of original draft. Yasong Li: supervision, writing including review and editing, and funding acquisition. Qichen Hao: conceptualization, validation, and writing including review and editing. Chunlei Liu: supervision, validation, and writing including review and editing. Yuchen Zhu: data curation, validation, and investigation. Zhenghong Li: data curation, investigation, and writing including review and editing. Ruoxi Yuan: data curation and writing including review and editing.

**Funding** This work was financially supported by the China Geological Survey Program (DD20190303, DD20221773), National Key Research and Development Program (2022YFF1301301), and Basic Research Funds for National Research Institutes (SK202114).

**Data availability** Most of data have been uploaded in the supplemental material. More detail data can be accessed from the authors by reasonable request.

## Declarations

**Ethics approval and consent to participate** Ethics approval is not applicable. The authors express their consent to have participated in the submitted work.

**Consent for publication** The authors state that the data used is in the public domain and may be published.

**Competing interests** The authors declare no competing interests.

## References

- Aleem M, Hoch G, Varner J (1965) Water as the source oxidant and reductant in bacterial chemosynthesis. *Proc Natl Acad Sci USA* 54:869–873
- Archana A, Thibodeau B, Geeraert N, Xu MN, Kao S-J, Baker DM (2018) Nitrogen sources and cycling revealed by dual isotopes of nitrate in a complex urbanized environment. *Water Res* 142:459–470
- Bernard-Jannin L, Sun X, Teissier S, Sauvage S, Sánchez-Pérez J-M (2017) Spatio-temporal analysis of factors controlling nitrate

- dynamics and potential denitrification hot spots and hot moments in groundwater of an alluvial floodplain. *Ecol Eng* 103:372–384
- Bertrand G, Petelet-Giraud E, Cary L, Hirata R, Montenegro S, Paiva A, Mahlkecht J, Coelho V, Almeida C (2022) Delineating groundwater contamination risks in southern coastal metropolises through implementation of geochemical and socio-environmental data in decision-tree and geographical information system. *Water Res* 209:117877
- Botero-Acosta A, Chu ML, Huang C (2019) Impacts of environmental stressors on nonpoint source pollution in intensively managed hydrologic systems. *J Hydrol* 579:124056
- Cao D, Cao W, Fang J, Cai L (2014) Nitrogen and phosphorus losses from agricultural systems in China: a meta-analysis. *Mar Pollut Bull* 85:727–732
- Cao W, Huang Z, Zhai W, Li Y, Hong H (2015) Isotopic evidence on multiple sources of nitrogen in the northern Jiulong River, Southeast China. *Estuar Coast Shelf Sci* 163:37–43
- Cao T, Han D, Song X, Trolle D (2020) Subsurface hydrological processes and groundwater residence time in a coastal alluvium aquifer: evidence from environmental tracers ( $\delta^{18}\text{O}$ ,  $\delta^2\text{H}$ , CFCs,  $^3\text{H}$ ) combined with hydrochemistry. *Sci Total Environ* 743:140684
- Cao S, Fei Y, Tian X, Cui X, Zhang X, Yuan R, Li Y (2021) Determining the origin and fate of nitrate in the Nanyang Basin, Central China, using environmental isotopes and the Bayesian mixing model. *Environ Sci Pollut Res* 28:48343–48361
- Casciotti KL (2016) Nitrogen and oxygen isotopic studies of the marine nitrogen cycle. *Ann Rev Mar Sci* 8:379–407
- Chang Y, Yin G, Hou L, Liu M, Zheng Y, Han P, Dong H, Liang X, Gao D, Liu C (2021) Nitrogen removal processes coupled with nitrification in coastal sediments off the north East China Sea. *J Soils Sediments* 21:3289–3299
- Cojean ANY, Zopfi J, Gerster A, Frey C, Lepori F, Lehmann M (2019) Direct O<sub>2</sub> control on the partitioning between denitrification and dissimilatory nitrate reduction to ammonium in lake sediments. *Biogeosciences* 16:4705–4718
- de la Reguera E, Tully KL (2021) Farming carbon: the link between saltwater intrusion and carbon storage in coastal agricultural fields. *Agr Ecosyst Environ* 314:107416
- Deutsch B, Mewes M, Liskow I, Voss M (2006) Quantification of diffuse nitrate inputs into a small river system using stable isotopes of oxygen and nitrogen in nitrate. *Org Geochem* 37:1333–1342
- Ding J, Xi B, Xu Q, Su J, Huo S, Liu H, Yu Y, Zhang Y (2015) Assessment of the sources and transformations of nitrogen in a plain river network region using a stable isotope approach. *J Environ Sci* 30:198–206
- DiSpirito AA, Hooper AB (1986) Oxygen exchange between nitrate molecules during nitrite oxidation by *Nitrobacter*. *J Biol Chem* 261:10534–10537
- Du Y, Ma T, Deng Y, Shen S, Lu Z (2017) Sources and fate of high levels of ammonium in surface water and shallow groundwater of the Jianghan Plain, Central China. *Environ Sci Process Impacts* 19:161–172
- Erostate M, Huneau F, Garel E, Lehmann MF, Kuhn T, Aquilina L, Vergnaud-Ayraud V, Labasque T, Santoni S, Robert S, Provotolo D, Pasqualini V (2018) Delayed nitrate dispersion within a coastal aquifer provides constraints on land-use evolution and nitrate contamination in the past. *Sci Total Environ* 644:928–940
- Frick H, Oberson A, Frossard E, Bünenmann EK (2022) Leached nitrate under fertilised loamy soil originates mainly from mineralisation of soil organic N. *Agr Ecosyst Environ* 338:108093
- Guo Z, Yan C, Wang Z, Xu F, Yang F (2020) Quantitative identification of nitrate sources in a coastal peri-urban watershed using hydrogeochemical indicators and dual isotopes together with the statistical approaches. *Chemosphere* 243:125364
- Guo J, Zuo P, Yang L, Pan Y, Wang L (2021) Quantitative identification of non-point sources of nitrate in urban channels based on dense in-situ samplings and nitrate isotope composition. *Chemosphere* 263:128219
- Hamilton SK (2012) Biogeochemical time lags may delay responses of streams to ecological restoration. *Freshw Biol* 57:43–57
- Han D, Currell MJ (2022) Review of drivers and threats to coastal groundwater quality in China. *Sci Total Environ* 806:150913
- Hu M, Liu Y, Zhang Y, Dahlgren RA, Chen D (2019) Coupling stable isotopes and water chemistry to assess the role of hydrological and biogeochemical processes on riverine nitrogen sources. *Water Res* 150:418–430
- Jacob J, Sanders T, Dähnke K (2016) Nitrite consumption and associated isotope changes during a river flood event. *Biogeosciences* 13:5649–5659
- Jiang Z, Wujin L, Zhiping L, Guizhang Z (2018) Indoor experiment and numerical simulation study of ammonia-nitrogen migration rules in soil column. *J Groundw Sci Eng* 6:205
- Jin Z, Zheng Q, Zhu C, Wang Y, Cen J, Li F (2018) Contribution of nitrate sources in surface water in multiple land use areas by combining isotopes and a Bayesian isotope mixing model. *Appl Geochem* 93:10–19
- Jun C, Ban Y, Li S (2014) Open access to Earth land-cover map. *Nature* 514:434–434
- Kendall C (1998) Chapter 16 - Tracing nitrogen sources and cycling in catchments. In: Kendall C, McDonnell JJ (eds) *Isotope tracers in catchment hydrology*. Elsevier, Amsterdam, pp 519–576
- Kendall C, Aravena R, Cook PG, Herczeg AL (2000) Nitrate Isotopes in Groundwater Systems. In: Cook PG, Herczeg AL (eds) *Environmental Tracers in Subsurface Hydrology*. Springer, US, Boston, MA, pp 261–297
- Kibuye FA, Gall HE, Veith TL, Elkin KR, Elliott HA, Harper JP, Watson JE (2020) Influence of hydrologic and anthropogenic drivers on emerging organic contaminants in drinking water sources in the Susquehanna River Basin. *Chemosphere* 245:125583
- Kim H, Kaown D, Mayer B, Lee J-Y, Hyun Y, Lee K-K (2015) Identifying the sources of nitrate contamination of groundwater in an agricultural area (Hae-an basin, Korea) using isotope and microbial community analyses. *Sci Total Environ* 533:566–575
- Kim SH, Lee DH, Kim MS, Rhee HP, Hur J, Shin KH (2023) Systematic tracing of nitrate sources in a complex river catchment: an integrated approach using stable isotopes and hydrological models. *Water Res* 235:119755
- Kwon E, Park J, Park W-B, Kang B-R, Woo NC (2021) Nitrate contamination of coastal groundwater: sources and transport mechanisms along a volcanic aquifer. *Sci Total Environ* 768:145204
- Li C, Li S-L, Yue F-J, Jing L, Zhong J, Yan Z, Zhang R-C, Zhongjun W, Xu S (2018) Identification of sources and transformations of nitrate in the Xijiang River using nitrate isotopes and Bayesian model. *Sci Total Environ* 646:801–810
- Li J, Zou S, Wang J, Zhou C, Wu Y, Zhang H, Zhao Y, Yang G (2023) Spatiotemporal variability and control factors of NO<sub>3</sub><sup>-</sup> in a polluted karst water system of an agricultural wetland in South China. *Chemosphere* 313:137435
- Li Y, Liu Y, Shi G, Liu C, Hao Q, Wu L (2022) Occurrence and risk assessment of perfluorooctanoate (PFOA) and perfluorooctane sulfonate (PFOS) in Surface water, groundwater and sediments of the Jin River Basin, Southeastern China. *B Environ Contam Tox* 108:1026–1032
- Meghdadi A, Javar N (2018) Evaluation of nitrate sources and the percent contribution of bacterial denitrification in hyporheic zone using isotope fractionation technique and multi-linear regression analysis. *J Environ Manage* 222:54–65
- Minet EP, Goodhue R, Meier-Augenstein W, Kalin RM, Fenton O, Richards KG, Coxon CE (2017) Combining stable isotopes with contamination indicators: a method for improved investigation of nitrate sources and dynamics in aquifers with mixed nitrogen inputs. *Water Res* 124:85–96
- Mohd Jani SJ, Toor G (2018) Composition, sources, and bioavailability of nitrogen in a longitudinal gradient from freshwater to estuarine waters. *Water Res* 137:344–354
- Moore JW, Semmens BX (2008) Incorporating uncertainty and prior information into stable isotope mixing models. *Ecol Lett* 11:470–480

- Nestler A, Berglund M, Accoe F, Duta S, Xue D, Boeckx P, Taylor P (2011) Isotopes for improved management of nitrate pollution in aqueous resources: review of surface water field studies. *Environ Sci Pollut Res Int* 18:519–533
- Ogrinc N, Tamšič S, Zavadlav S, Vrzel J, Jin L (2019) Evaluation of geochemical processes and nitrate pollution sources at the Ljubljansko polje aquifer (Slovenia): a stable isotope perspective. *Sci Total Environ* 646:1588–1600
- Parnell AC, Phillips DL, Bearhop S, Semmens BX, Ward EJ, Moore JW, Jackson AL, Grey J, Kelly DJ, Inger R (2013) Bayesian stable isotope mixing models. *Environmetrics* 24:387–399
- Phillips DL, Gregg JW (2003) Source partitioning using stable isotopes: coping with too many sources. *Oecologia* 136:261–269
- Qiao Z, Sun R, Wu Y, Hu S, Liu X, Chan J, Mi X (2020) Characteristics and metabolic pathway of the bacteria for heterotrophic nitrification and aerobic denitrification in aquatic ecosystems. *Environ Res* 191:110069
- Qiu ZK, Hu XZ, Yao C, Zhang WH, Xu QJ, Huang TY (2016) Pollution characteristics and evaluation of nitrogen, phosphorus and organic matter in sediments of Shanmei Reservoir in Fujian, China. *Environmetal Science* 37:1389–1396
- Ren K, Pan X, Yuan D, Zeng J, Liang J, Peng C (2022) Nitrate sources and nitrogen dynamics in a karst aquifer with mixed nitrogen inputs (Southwest China): revealed by multiple stable isotopic and hydro-chemical proxies. *Water Res* 210:118000
- Richards G, Gilmore TE, Mittelstet AR, Messer TL, Snow DD (2021) Baseflow nitrate dynamics within nested watersheds of an agricultural stream in Nebraska, USA. *Agr Ecosyst Environ* 308:107223
- Sigman D, Casciotti K, Andreani M, Barford C, Hastings M, Bohlke J (2001) A bacterial method for the nitrogen isotopic analysis of nitrate in seawater and freshwater. *Anal Chem* 73:4145–4153
- Soto DX, Koehler G, Wassenaar LI, Hobson KA (2019) Spatiotemporal variation of nitrate sources to Lake Winnipeg using N and O isotope ( $\delta^{15}\text{N}$ ,  $\delta^{18}\text{O}$ ) analyses. *Sci Total Environ* 647:486–493
- Spalding R, Hirsh A, Exner M, Stange M, Aravena R (2018) Integrated deep soil N and groundwater isotope investigation of N sources captured by municipal wells. *Groundwater Monit Remediat* 39(2):22–31
- Stock B, Semmens B, Ward E, Moore J, Parnell A, Jackson A, Phillips D, Bearhop S, Inter R (2014) MixSIAR: advanced stable isotope mixing models in R. Presented at Ecological Society of America, Sacramento, CA
- Torres-Martínez JA, Mora A, Mählknecht J, Daesslé LW, Cervantes-Avilés PA, Ledesma-Ruiz R (2021) Estimation of nitrate pollution sources and transformations in groundwater of an intensive livestock-agricultural area (Comarca Lagunera), combining major ions, stable isotopes and MixSIAR model. *Environ Pollut* 269:115445
- Valiente N, Gil Márquez J, Gómez-Alday JJ, Andreo B (2020) Unraveling groundwater functioning and nitrate attenuation in evaporitic karst systems from southern Spain: an isotopic approach. *Appl Geochem* 123:104820
- Van Drecht G, Bouwman AF, Harrison J, Knoop JM (2009) Global nitrogen and phosphate in urban wastewater for the period 1970 to 2050. *Global Biogeochem Cycles* 23
- Van Meter KJ, Van Cappellen P, Basu NB (2018) Legacy nitrogen may prevent achievement of water quality goals in the Gulf of Mexico. *Science* 360:427–430
- Voss M, Deutsch B, Elmgren R, Humborg C, Kuuppo P, Pastuszak M, Rolff C, Schulte U (2006) River biogeochemistry and source identification of nitrate by means of isotopic tracers in the Baltic Sea catchments. Copernicus GmbH, pp. 475–511
- Wang P, Zhang F, Chen Z (2020) Characterization of recharge processes and groundwater flow paths using isotopes in the arid Santanghu basin, Northwest China. *Hydrogeol J* 28(1037):1051
- Weitzman JN, Brooks JR, Compton JE, Faulkner BR, Mayer PM, Peachey RE, Rugh WD, Coulombe RA, Hatteberg B, Hutchins SR (2022) Deep soil nitrogen storage slows nitrate leaching through the vadose zone. *Agr Ecosyst Environ* 332:107949
- Wu G, Cao W, Huang Z, Kao C-M, Chang C-T, Chiang P-C, Wang F (2017) Decadal changes in nutrient fluxes and environmental effects in the Jiulong River Estuary. *Mar Pollut Bull* 124:871–877
- Xu H, Gao Q, Yuan B (2022) Analysis and identification of pollution sources of comprehensive river water quality: evidence from two river basins in China. *Ecol Ind* 135:108561
- Xue D, Botte J, De BB, Accoe F, Nestler A, Taylor P, Van CO, Berglund M, Boeckx P (2009) Present limitations and future prospects of stable isotope methods for nitrate source identification in surface and groundwater. *Water Res* 43:1159–1170
- Xue D, Boeckx P, Wang Z (2014) Nitrate sources and dynamics in a salinized river and estuary - a  $\delta^{15}\text{N}\text{-NO}_3^-$  and  $\delta^{18}\text{O}\text{-NO}_3^-$  isotope approach. *Biogeosciences* 11:5957–5967
- Yan W, Mayorga E, Li X, Seitzinger SP, Bouwman AF (2010) Increasing anthropogenic nitrogen inputs and riverine DIN exports from the Changjiang River basin under changing human pressures. *Glob Biogeochem Cycles* 24
- Yang Y-Y, Toor GS (2016)  $\delta^{15}\text{N}$  and  $\delta^{18}\text{O}$  reveal the sources of nitrate-nitrogen in urban residential stormwater runoff. *Environ Sci Technol* 50:2881–2889
- Yang L, Han J, Xue J, Zeng L, Shi J, Wu L, Jiang Y (2013) Nitrate source apportionment in a subtropical watershed using Bayesian model. *Sci Total Environ* 463-464C:340–347
- Yang P, Lai DYF, Jin B, Bastviken D, Tan L, Tong C (2017) Dynamics of dissolved nutrients in the aquaculture shrimp ponds of the Min River estuary, China: concentrations, fluxes and environmental loads. *Sci Total Environ* 603–604:256–267
- Yang L, FengXin K, Ande Z (2019) Isotope analysis of nitrate pollution sources in groundwater of Dong'e geohydrological unit. *J Groundw Sci Eng* 7:145
- Ye F, Guo W, Shi Z, Jia G, Wei G (2017) Seasonal dynamics of particulate organic matter and its response to flooding in the Pearl River Estuary, China, revealed by stable isotope ( $\delta^{13}\text{C}$  and  $\delta^{15}\text{N}$ ) analyses. *J Geophys Res Oceans* 122:6835–6856
- Yi Q, Chen Q, Hu L, Shi W (2017) Tracking nitrogen sources, transformation, and transport at a basin scale with complex plain river networks. *Environ Sci Technol* 51:5396–5403
- Yu D, Yan W, Chen N, Peng B, Hong H, Zhuo G (2015) Modeling increased riverine nitrogen export: source tracking and integrated watershed-coast management. *Mar Pollut Bull* 101:642–652
- Yu Q, Wang F, Li X, Yan W, Li Y, Lv S (2018) Tracking nitrate sources in the Chaohu Lake, China, using the nitrogen and oxygen isotopic approach. *Environ Sci Pollut Res* 25:19518–19529
- Yu J, Zhang W, Tan Y, Zong Z, Hao Q, Tian C, Zhang H, Li J, Fang Y, Zhang G (2021) Dual-isotope-based source apportionment of nitrate in 30 rivers draining into the Bohai Sea, North China. *Environ Pollut* 283:117112
- Zhang Y, Shi P, Li F, Wei A, Song J, Ma J (2018) Quantification of nitrate sources and fates in rivers in an irrigated agricultural area using environmental isotopes and a Bayesian isotope mixing model. *Chemosphere* 208:493–501

**Publisher's note** Springer Nature remains neutral with regard to jurisdictional claims in published maps and institutional affiliations.

Springer Nature or its licensor (e.g. a society or other partner) holds exclusive rights to this article under a publishing agreement with the author(s) or other rightsholder(s); author self-archiving of the accepted manuscript version of this article is solely governed by the terms of such publishing agreement and applicable law.